SIAM J. APPL. MATH.
Vol. 81, No. 3, pp. 1098–1115

A GENERALIZED RAYLEIGH–PLESSET EQUATION FOR IONS WITH SOLVENT FLUCTUATIONS*

CHAO FAN†, BO LI‡, AND MICHAEL R. WHITE§

Abstract. We introduce a mathematical modeling framework for the conformational dynamics of charged molecules (i.e., solutes) in an aqueous solvent (i.e., water or salted water). The solvent is treated as an incompressible fluid, and its fluctuating motion is described by the Stokes equation with the Landau–Lifschitz stochastic stress. The motion of the solute-solvent interface (i.e., the dielectric boundary) is determined by the fluid velocity together with the balance of the viscous force, hydrostatic pressure, surface tension, solute-solvent van der Waals interaction force, and electrostatic force. The electrostatic interactions are described by the dielectric Poisson–Boltzmann theory. Within such a framework, we derive a generalized Rayleigh–Plesset equation, a nonlinear stochastic ordinary differential equation (SODE), for the radius of a spherical charged molecule, such as an ion. The spherical average of the stochastic stress leads to a multiplicative noise. We design and test numerical methods for solving the SODE and use the equation, together with explicit-solvent molecular dynamics simulations, to study the effective radius of a single ion. Potentially, our general modeling framework can be used to efficiently determine the solute-solvent interfacial structures and predict the free energies of more complex molecular systems.

Key words. charged molecules, solute-solvent interface, Stokes equation, Landau–Lifschitz stochastic stress tensor, Poisson–Boltzmann equation, generalized Rayleigh–Plesset equation

AMS subject classifications. 60H10, 60H35, 65C30, 76D07, 92C05

DOI. 10.1137/20M1360268

1. Introduction.

We study the conformational dynamics of charged molecules (e.g., an ion or a protein) in an aqueous solvent (i.e., water or salted water), aiming at understanding the role of the solvent viscosity and solvent fluctuations in such dynamics [2, 4, 17, 20, 22, 25, 39, 46]. We introduce a mathematical modeling framework with a dynamic implicit solvent to describe such a role. Here, an implicit solvent means a continuum solvent; i.e., the solvent is treated as a continuum rather through individual solvent molecules. Within such a framework, we derive a stochastic ordinary differential equation (SODE) and study the effective radius of a single ion.

Our modeling framework is a combination of a static variational model [15, 52, 53] and a stochastic fluid mechanics approach [24]. In the variational model, one minimizes a macroscopic solvation free-energy functional $G[\Gamma]$ among all the possible solute-solvent interfaces (i.e., dielectric boundaries) Γ that are closed surfaces enclosing all the solute atoms located at $\mathbf{x}_1, \ldots, \mathbf{x}_N$ inside the solvation region Ω; cf. Figure 1. A solute-solvent interface Γ separates the solute region $\Omega_{\rm p}$ (p stands for

*Received by the editors August 17, 2020; accepted for publication (in revised form) March 12, 2021; published electronically June 3, 2021.
https://doi.org/10.1137/20M1360268
Funding: The work of the second author was partially supported by the U.S. National Science Foundation through grant DMS-1913144, by the U.S. National Institutes of Health through grant R01GM132106, and by a 2019–2020 Lattimer Faculty Research Fellowship, Division of Physical Sciences, University of California, San Diego. The work of the third author was supported by a University of California Office of President Computational Science Graduate Fellowship.

†Department of Mathematics, University of California, San Diego, CA 92093-0112 USA (chf004@ucsd.edu).
‡Department of Mathematics and Quantitative Biology Ph.D. Program, University of California, San Diego, CA 92093-0112 USA (bli@math.ucsd.edu).
§School of Mathematics, University of Minnesota, Minneapolis, MN 55455 USA (mwhite85@gmail.com).

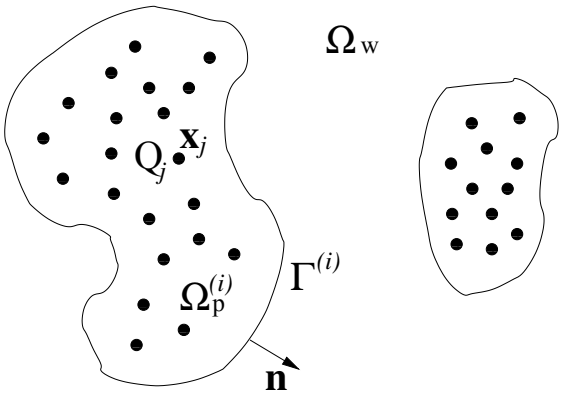

FIG. 1. *A schematic diagram of charged molecules immersed in an aqueous solvent. The region of solvation Ω is divided into the solvent region Ω_w, the solute region $\Omega_p = \cup_{i=1}^m \Omega_p^{(i)}$, and the solute-solvent interface (i.e., the dielectric boundary) $\Gamma = \cup_{i=1}^m \Gamma^{(i)}$, where $\Omega_p^{(i)}$ is a connected component of Ω_p and $\Gamma^{(i)} = \partial\Omega_p^{(i)}$ is the boundary of $\Omega_p^{(i)}$. The solute region Ω_p contains all the solute atoms $\mathbf{x}_j$ carrying partial charges Q_j $(j = 1, \ldots, N)$, with each component $\Omega_p^{(i)}$ containing N_i atoms. The unit vector $\mathbf{n}$ normal to Γ points from Ω_p to Ω_w.*

protein) from the solvent region $\Omega_{\rm w}$ (w stands for water). Both the solvent and solutes are approximated as dielectric media with different dielectric constants. The solvation free-energy functional consists of the energy needed to create the solute region $\Omega_{\rm p}$, the solute-solvent interfacial energy, the solute-solvent van der Waals (vdW) interaction energy, and the dielectric electrostatic energy determined by the dielectric Poisson–Boltzmann (PB) theory [8, 13, 26, 40]; cf. (2.1).

In the dynamic implicit-solvent model, all $\Omega_{\rm w} = \Omega_{\rm w}(t)$, $\Omega_{\rm p} = \Omega_{\rm p}(t)$, and $\Gamma = \Gamma(t)$ depend on time t. The motion of the solute-solvent interface $\Gamma(t)$, the key variable in the model, is governed by its normal velocity $V_n = \mathbf{u} \cdot \mathbf{n}$, where $\mathbf{n} = \mathbf{n}(\mathbf{x}, t)$ is the unit normal at the interface and $\mathbf{u} = \mathbf{u}(\mathbf{x}, t)$ is the solvent velocity field. The solvent fluid is incompressible, as it is mainly water, and the velocity field of the solvent fluid is governed by the stochastic Navier–Stokes equation (NSE) [24]

$$\rho_{\rm w}(\partial_t \mathbf{u} + \mathbf{u} \cdot \nabla \mathbf{u}) = \mu_{\rm w} \nabla^2 \mathbf{u} - \nabla P_{\rm w} + \mathbf{F}_{\rm ext} + \nabla \cdot \mathbf{\Sigma} \qquad \text{in } \Omega_{\rm w}(t),$$

where $\rho_{\rm w}$ is the constant fluid density, $\mu_{\rm w}$ the dynamic viscosity, $P_{\rm w}$ the solvent fluid pressure, $\mathbf{F}_{\rm ext}$ an external force, and $\mathbf{\Sigma}$ the Landau–Lifshitz stochastic stress tensor. Since the fluid motion at the molecular scale is friction dominated, we can neglect the inertia term in the NSE and consider alternatively the stochastic Stokes equation for the fluid velocity field. The force balance leads to the interface condition

$$2\mu_{\rm w} \mathbf{D}(\mathbf{u})\mathbf{n} - \delta_\Gamma G[\Gamma]\mathbf{n} = \mathbf{0} \qquad \text{on } \Gamma(t),$$

where $\mathbf{D}(\mathbf{u})$ is the strain-rate tensor and $-\delta_\Gamma G[\Gamma]\mathbf{n}$ is the conserved force arising from the free energy $G[\Gamma]$ of the dielectric boundary Γ in the variational model, where δ_Γ denotes the variational derivative; see section 2 for more details.

With the dynamic implicit-solvent modeling framework, we derive a generalized Rayleigh–Plesset (RP) equation for the radius $R = R(t)$ of a spherical charged solute, such as an ion. We recall the classical RP equation for the radius of spherical bubble

in a fluid [33, 34, 36]

$$R\ddot{R} + \frac{3}{2}\dot{R}^2 + \frac{4\mu_{\rm w}}{\rho_{\rm w}R}\dot{R} + \frac{2\gamma_0}{\rho_{\rm w}R} = \frac{P_{\rm w} - P_\infty}{\rho_{\rm w}},$$

where P_∞ is the pressure at infinity and γ_0 is the surface tension of the air-fluid interface. The RP equation has been used extensively in the study of bubble dynamics [5, 14, 18, 29, 33, 34, 36]. Our generalized RP equation is a nonlinear SODE with a multiplicative noise that results from the spherical average of the Landau–Lifschitz stochastic stress. The equation couples different kinds of forces, particularly the electrostatic force, in the motion of the spherical molecule. There are three versions of our generalized RP equation, corresponding to the full NSE, the time-dependent Stokes equation, and the time-independent Stokes equation, respectively; cf. Theorem 3.1. We design and test numerical methods for solving the generalized RP equation and, with the help of explicit-water molecular dynamics (MD) simulations, study the effective radius of a single ion through the solvent radial distribution.

We remark that in practice, the Stokes equation should be suitable, as the inertia of a molecular fluid is weak and can be neglected. However, we consider the full NSE so that we can compare our generalized RP equation with the classical RP equation. Moreover, we will see how some numerical scheme for the generalized RP equation can be simplified.

The variational implicit-solvent model, which is a key component of the force modeling in the dynamic implicit-solvent model, has been successful in providing reasonable estimations of the free energy of molecular solvation, describing the strong effect of electrostatic interactions, and capturing the multiple dry and wet solvation states; cf., e.g., [10, 11, 49, 52]. In the recent work [53], the authors combine the variational solvation model, the string method for minimum energy paths, and the state-dependent Brownian dynamics simulations and Fokker–Planck equations to predict the kinetics of molecular binding and unbinding processes, showing new potentials of the variational implicit solvation approach.

In recent years, there has been a growing interest in modeling the conformation and dynamics of charged molecules in an aqueous solvent using the continuum fluid mechanics theory [16, 28, 50, 51]. Naturally, one questions the validity of such a theory, the NSE or Stokes equation specifically, applied to a molecular solvation system of nanoscale length. For instance, the density and viscosity of solvent molecules around the solutes, if properly defined, are presumably rather inhomogeneous. Therefore, one will not expect to capture any molecular details, such as water orientations, hydration shells around proteins, and the kinetics of water molecules moving through a carbon nanotube, by using a continuum, fluid mechanics equation. However, just like the dielectric PB model for protein electrostatics, a solvent fluid model, which is expected to be still much more efficient than all-atom MD simulations, can potentially describe some mesoscopic properties of solvent with bulk values of solvent density and viscosity. This is in alignment with experiments on adjusting the bulk solvent viscosity to investigate its effect to the kinetics of conformational change of macromolecules [2, 4, 17, 39]. With the inclusion of stochastic stress, a solvent fluid model may better describe the effect of the mean viscous force on the solute-solvent interfacial structures and better capture the transition between different metastable states [25, 32].

Our solvent fluid model is first developed in [50, 51], where no stochastic stress is included. The treatment of electrostatics using the dielectric boundary force is proposed in [50], and some statistical mechanics basis of the model is provided in [51]. In [28], the authors perform a linear stability analysis to show the stability and in-

stability of a cylindrical solute-solvent equilibrium interface under the influence of all the forces and find the key parameter to be the ratio of the surface tension and the viscosity. Sun et al. [44, 45] develop numerical methods to implement the dynamic implicit-solvent model without fluctuations but with special numerical boundary conditions that allow the solvent to flow in and out of the computational region to capture different dry and wet solvation states.

In section 2, we first review the static variational implicit-solvent model for molecular solvation. We then present the dynamic implicit-solvent model as a general mathematical modeling framework for the description of the solvent fluid motion with fluctuations and the conformational dynamics of charged molecules. In section 3, we apply our modeling framework to a spherical charged molecule in an aqueous solvent and derive the generalized RP equation for the fluctuating motion of the sphere. In section 4, we describe our numerical methods for solving the generalized RP equation and present the related numerical results. In section 5, we apply our generalized RP equation together with MD simulations to study the effective radius of a single ion. Finally, in section 6, we briefly draw conclusions and discuss several modeling issues and our future work.

2. A dynamic implicit-solvent modeling framework. We consider a solvation system of charged molecules immersed in an aqueous solvent as illustrated by Figure 1. Note that we use the solute-solvent interface Γ as a dielectric boundary since the dielectric coefficient of the solvent, $\varepsilon_{\rm w}$, is in general much larger than that of the solutes, $\varepsilon_{\rm p}$. We define $\varepsilon_\Gamma : \Omega \to \mathbb{R}$ by

$$\varepsilon_\Gamma(\mathbf{x}) = \begin{cases} \varepsilon_{\rm p} & \text{if } \mathbf{x} \in \Omega_{\rm p}, \\ \varepsilon_{\rm w} & \text{if } \mathbf{x} \in \Omega_{\rm w}. \end{cases}$$

We recall the solvation free-energy functional $G = G[\Gamma]$ in the variational implicit-solvent model [12, 15, 49, 52], where Γ is a solute-solvent interface (cf. Figure 1):

$$G[\Gamma] = (P_{\rm w} - P_{\rm p})\,\mathrm{vol}(\Omega_{\rm p}) + \gamma_0 \int_\Gamma (1 - 2\tau H)\, dS + n_{\rm w} \int_{\Omega_{\rm w}} U_{\rm vdW}\, dV + G_{\rm elec}[\Gamma]. \tag{2.1}$$

Here, the first term is the work to create the solute region $\Omega_{\rm p}$, where $P_{\rm w}$ and $P_{\rm p}$ are the solvent pressure and solute pressure, respectively. The second term is the surface energy, in which γ_0 is the constant surface tension, H the mean curvature, and τ a constant correction parameter often called the Tolman length [47]. The third term, in which $n_{\rm w}$ is the solvent number density, describes the solute-solvent vdW interactions. The potential function $U_{\rm vdW}$ is given by $U_{\rm vdW}(\mathbf{x}) = \sum_{i=1}^N U_{\rm LJ}^{(i)}\left(|\mathbf{x} - \mathbf{x}_i|\right)$, where each $U_{\rm LJ}^{(i)}$ is a 12-6 Lennard-Jones (LJ) potential

$$U_{\rm LJ}^{(i)}(r) = 4\varepsilon_i \left[\left(\frac{\sigma_i}{r}\right)^{12} - \left(\frac{\sigma_i}{r}\right)^{6} \right] \tag{2.2}$$

with ε_i and σ_i the energy and length parameters.

The last term $G_{\rm elec}[\Gamma]$ in (2.1) is the electrostatic part of the free energy. Within the PB theory [8, 13, 26, 40, 52], it is given by

$$G_{\rm elec}[\Gamma] = \frac{1}{2}\sum_{i=1}^N Q_i(\psi - \psi_{\rm ref})(\mathbf{x}_i) - \frac{1}{2}\int_{\Omega_{\rm w}} \psi B'(\psi)\, dV - \int_{\Omega_{\rm w}} B(\psi)\, dV. \tag{2.3}$$

Here, the electrostatic potential ψ is determined by the PB equation (cf. (2.12) below) together with some boundary conditions, $\psi_{\rm ref}(\mathbf{x}) = \sum_{i=1}^{N} Q_i/(4\pi\varepsilon_0\varepsilon_{\rm p}|\mathbf{x}-\mathbf{x}_i|)$ is a reference field with ε_0 the vacuum permittivity, and

$$B(\psi) = k_{\rm B}T\sum_{i=1}^{M} c_i^{\infty}\left(e^{-q_i\psi/k_{\rm B}T}-1\right) \tag{2.4}$$

with $k_{\rm B}$ the Boltzmann constant, T temperature, and c_i^{∞} and q_i the bulk concentration and charge of ions of the ith species (a total of M species assumed), respectively. As usual, we assume the ionic charge neutrality

$$\sum_{i=1}^{M} c_i^{\infty} q_i = 0. \tag{2.5}$$

The negative first variation of the $G[\Gamma]$ defines the normal component of the boundary force on Γ. It is given by [6, 7, 8, 27, 52]

$$\begin{aligned} -\delta_\Gamma G[\Gamma] = {} & P_{\rm p} - P_{\rm w} - 2\gamma_0(H-\tau K) + n_{\rm w}U_{\rm vdW} + \frac{1}{2}\left(\frac{1}{\varepsilon_{\rm w}\varepsilon_0}-\frac{1}{\varepsilon_{\rm p}\varepsilon_0}\right)|\varepsilon_\Gamma\nabla\psi\cdot\mathbf{n}|^2 \\ & + \frac{1}{2}(\varepsilon_{\rm p}\varepsilon_0-\varepsilon_{\rm w}\varepsilon_0)|(\mathbf{I}-\mathbf{n}\otimes\mathbf{n})\nabla\psi|^2 - B(\psi) \qquad \text{on } \Gamma, \end{aligned} \tag{2.6}$$

where K is the Gaussian curvature and $\mathbf{I}$ the identity tensor. The linear PB equation for the electrostatic potential, the corresponding electrostatic energy, and the corresponding dielectric boundary force have all the same expressions but with the following linearized version of $B(\psi)$:

$$B(\psi) = \frac{1}{2}\varepsilon_{\rm w}\varepsilon_0\kappa^2\psi^2 \qquad \text{with} \quad \kappa = \sqrt{\frac{1}{\varepsilon_{\rm w}\varepsilon_0 k_{\rm B}T}\sum_{i=1}^{M} c_i^{\infty}q_i^2}. \tag{2.7}$$

The parameter κ is the inverse Debye length.

We now consider the dynamics of our molecular system and assume thus that all $\Omega_{\rm w}$, $\Omega_{\rm p}$, $\Omega_{\rm p}^{(i)}$, Γ, and $\Gamma^{(i)}$ depend on time t. Note that the number of solute components m can now also depend on t. The main elements of our dynamic implicit-solvent model are as follows:

(1) The motion of the dielectric boundary $\Gamma(t)$ is determined by its normal velocity $V_n(\mathbf{x}) = \dot{\mathbf{x}}\cdot\mathbf{n}(\mathbf{x})$ for any $\mathbf{x} = \mathbf{x}(t) \in \Gamma(t)$, where a dot on top denotes the time derivative. We model the normal velocity V_n of the dielectric boundary to be the same as the normal component of the solvent fluid velocity $\mathbf{u} = \mathbf{u}(\mathbf{x})$ at the boundary [3, 24, 31].

(2) The solvent fluid is incompressible, as the solvent in a biological molecular system is often water or salted water with low salt concentrations. The solvent fluid motion is described by the NSE or by the Stokes equation, as the fluid is friction dominated [3, 24, 31]. Moreover, the solvent fluctuation is described by the Landau–Lifshitz stochastic stress tensor [24].

(3) The pressure $P = P(\mathbf{x}, t)$ is defined in the entire solvation region Ω as follows:

$$P(\mathbf{x},t) = \begin{cases} P_{\rm w}(\mathbf{x},t) & \text{if } \mathbf{x}\in\Omega_{\rm w}(t), \\ P_{\rm p}(t) = P_{\rm p}^{(i)}(t) & \text{if } \mathbf{x}\in\Omega_{\rm p}^{(i)}(t) \quad (i=1,\ldots,m(t)). \end{cases}$$

In each of the solute subregions $\Omega_{\rm p}^{(i)}(t)$ $(1 \le i \le m(t))$, the pressure $P_{\rm p}^{(i)}(t)$ is approximated to be spatially constant, and the ideal-gas law applies.

(4) The electrostatic interactions among the partial charges Q_j carried by solute atoms located at $\mathbf{x}_j$ $(j = 1, \ldots, N)$, mobile ions in the solvent, and polarized solvent medium are described by the PB equation (nonlinear or linear) [8, 13, 26, 40] and the dielectric boundary force [6, 7, 8, 9, 27].

(5) At the solute-solvent interface $\Gamma(t)$, the viscous force, hydrostatic pressure, solute-solvent vdW interaction force, surface tension (which includes the Tolman correction), and electrostatic force are all balanced. This means that the interface equilibrates locally much faster than the averaged solvent fluid motion.

The entire set of governing equations for the motion of solute-solvent interface $\Gamma(t)$, the velocity $\mathbf{u}$, the pressure P, and the electrostatic potential ψ are given by

$$V_n = \mathbf{u}\cdot\mathbf{n} \qquad \text{on } \Gamma(t), \tag{2.8}$$

Interface motion

$$\nabla\cdot\mathbf{u} = 0 \qquad \text{in } \Omega_{\mathrm{w}}(t), \tag{2.9}$$

Incompressibility

Stochastic NSE

$$\rho_{\mathrm{w}}(\partial_t\mathbf{u} + \mathbf{u}\cdot\nabla\mathbf{u}) = \mu_{\mathrm{w}}\nabla^2\mathbf{u} - \nabla P_{\mathrm{w}} + \mathbf{F}_{\mathrm{ext}} + \nabla\cdot\boldsymbol{\Sigma} \qquad \text{in } \Omega_{\mathrm{w}}(t), \tag{2.10}$$

$$P_{\mathrm{p}}^{(i)}(t) = \frac{N_i(t)\,k_{\mathrm{B}}T}{\mathrm{vol}(\Omega_{\mathrm{p}}^{(i)}(t))} \qquad \text{in } \Omega_{\mathrm{p}}^{(i)}(t) \ \ (i = 1, \ldots, m(t)), \tag{2.11}$$

Ideal-gas law

$$\nabla\cdot\varepsilon_{\Gamma(t)}\varepsilon_0\nabla\psi - \chi_{\Omega_{\mathrm{w}}(t)}B'(\psi) = -\sum_{j=1}^{N} Q_j\delta_{\mathbf{x}_j} \qquad \text{in } \Omega, \tag{2.12}$$

PBE

$$2\mu_{\mathrm{w}}\mathbf{D}(\mathbf{u})\mathbf{n} - \delta_\Gamma G[\Gamma]\mathbf{n} = \mathbf{0} \qquad \text{on } \Gamma(t). \tag{2.13}$$

Force balance

Alternatively, we can use the stochastic Stokes equation, time dependent or not, instead of the full stochastic NSE (2.10):

$$\rho_{\mathrm{w}}\partial_t\mathbf{u} = \mu_{\mathrm{w}}\nabla^2\mathbf{u} - \nabla P_{\mathrm{w}} + \mathbf{F}_{\mathrm{ext}} + \nabla\cdot\boldsymbol{\Sigma} \qquad \text{in } \Omega_{\mathrm{w}}(t), \tag{2.14}$$

$$\mu_{\mathrm{w}}\nabla^2\mathbf{u} - \nabla P_{\mathrm{w}} + \mathbf{F}_{\mathrm{ext}} + \nabla\cdot\boldsymbol{\Sigma} = \mathbf{0} \qquad \text{in } \Omega_{\mathrm{w}}(t). \tag{2.15}$$

Practically, the stochastic time-independent Stokes equation is preferred, as for a system at molecular scale, the inertia is weak and can be neglected.

In (2.10), (2.14), and (2.15), ρ_{w} is the constant solvent fluid density, μ_{w} the constant dynamic viscosity of the solvent fluid, and $\mathbf{F}_{\mathrm{ext}} = \mathbf{F}_{\mathrm{ext}}(\mathbf{x}, t)$ the density of an external force (e.g., applied shear per unit volume). The term $\nabla\cdot\boldsymbol{\Sigma}$ in these equations is the random force in the solvent fluid. The Landau–Lifshitz stochastic stress tensor $\boldsymbol{\Sigma} = \boldsymbol{\Sigma}(\mathbf{x}, t)$ is assumed to be a random Gaussian field with zero mean and covariance tensor given by [24]

$$\langle\boldsymbol{\Sigma}_{ij}(\mathbf{x}, t)\boldsymbol{\Sigma}_{k\ell}(\mathbf{x}', t')\rangle = 2\,\mu_{\mathrm{w}}\,k_B\,T\,\delta(\mathbf{x} - \mathbf{x}')\,\delta(t - t')\,(\delta_{ik}\delta_{j\ell} + \delta_{i\ell}\delta_{jk})\,, \tag{2.16}$$

where $\boldsymbol{\Sigma}_{ij}(\mathbf{x}, t)$ $(i, j = 1, 2, 3)$ are the components (in the Cartesian coordinates) of the tensor $\boldsymbol{\Sigma}(\mathbf{x}, t)$, δ is the Dirac delta function, and δ_{ij} is the Kronecker symbol: $\delta_{ij} = 1$ if $i = j$ and 0 if $i \neq j$. Note that, due to the fluid incompressibility, the form of the covariance tensor given here simplifies the general Landau–Lifshitz formula of such a tensor. In (2.11), $N_i(t)$ is the number of solute particles in the subregion $\Omega_{\mathrm{p}}^{(i)}(t)$. In (2.12), the function $\chi_{\Omega_{\mathrm{w}}(t)}(\mathbf{x})$ is the characteristic function of the solvent region $\Omega_{\mathrm{w}}(t)$. The symbol $\delta_{\mathbf{x}_i}$ denotes the Dirac delta function at $\mathbf{x}_i$. Note that the function $B(\psi)$ is defined in (2.4) and (2.7) for the nonlinear and linear PB equations, respectively. Note also that the dependence on t of the electrostatic potential $\psi(\mathbf{x}, t)$ is through

that of the dielectric boundary $\Gamma(t)$. Finally, in the force balance (2.13) [21, 24, 35], $\mathbf{D}(\mathbf{u}) = (\nabla\mathbf{u} + \nabla\mathbf{u}^T)/2$ (with a superscript T denoting the matrix transpose) is the strain-rate tensor, and $-\delta_\Gamma G[\Gamma]$ is given in (2.6).

To uniquely determine the velocity field $\mathbf{u}$ and electrostatic potential ψ, we need to specify their boundary conditions. If $\Omega = \mathbb{R}^3$ is the entire space, then we can set $\mathbf{u} = \mathbf{0}$ and $\psi = 0$ at infinity. If Ω is a bounded region, then the boundary condition for $\mathbf{u}$ needs to be set carefully in order to allow the change of volumes of $\Omega_{\rm p}^{(i)}$ $(i = 1, \ldots, m)$ [44]. The boundary condition for ψ can be $\psi = \psi_0$ on the boundary of Ω for some given potential ψ_0 [52].

3. A generalized RP equation. We now consider a spherical solute of radius $R = R(t)$ at time t, carrying a single point charge Q at its center that is assumed to be the origin of $\mathbb{R}^3$. The region of solvation is $\Omega = \mathbb{R}^3$. In the spherical coordinates, the dielectric boundary $\Gamma(t)$, solute region $\Omega_{\rm p}(t)$, and solvent region $\Omega_{\rm w}(t)$ are defined by $r = R(t)$, $r < R(t)$, and $r > R(t)$, respectively, where $r = |\mathbf{r}|$ and $\mathbf{r} = (x, y, z) \in \mathbb{R}^3$. Since there is $N = 1$ solute atom, we denote $U_{\rm LJ} = U_{\rm LJ}^{(1)}$, $\varepsilon = \varepsilon_1$, and $\sigma = \sigma_1$ (cf. (2.2)); i.e., we set

$$U_{\rm LJ}(r) = 4\varepsilon\left[\left(\frac{\sigma}{r}\right)^{12} - \left(\frac{\sigma}{r}\right)^{6}\right]. \tag{3.1}$$

We shall assume that the external force in (2.10)–(2.15) arises from a potential $U_{\rm ext}$, i.e.,

$$\mathbf{F}_{\rm ext} = -n_{\rm w}\nabla U_{\rm ext} \qquad \text{with} \quad U_{\rm ext}(\infty) = 0. \tag{3.2}$$

We define

$$F(R) = P_{\rm p}(R) - P_\infty - 2\gamma_0\left(\frac{1}{R} - \frac{\tau}{R^2}\right) + n_{\rm w}\left[U_{\rm LJ}(R) + U_{\rm ext}(R)\right] + f_{\rm elec}(R), \tag{3.3}$$

$$P_{\rm p}(R) = \frac{3k_{\rm B}T}{4\pi R^3}, \tag{3.4}$$

$$f_{\rm elec}(R) = \frac{Q^2}{32\pi^2\varepsilon_0}\left[\left(\frac{1}{\varepsilon_{\rm w}} - \frac{1}{\varepsilon_{\rm p}}\right)\frac{1}{R^4} - \frac{\kappa^2}{\varepsilon_{\rm w}(1+\kappa R)^2R^2}\right]. \tag{3.5}$$

Our main result in this section is the following.

THEOREM 3.1. *Assume that the velocity* $\mathbf{u}$*, pressure* P*, and electrostatic potential* ψ *are all spherically symmetric and satisfy* (2.8)–(2.13) (*with* (2.14) *or* (2.15) *replacing* (2.10) *alternatively and with the linear PB equation*)*, together with the boundary conditions that* $\mathbf{u}$*,* $\mathbf{\Sigma}$*, and* ψ *vanish at the infinity but* $P = P_\infty$ *at the infinity with* P_∞ *a given constant. Assume the stochastic stress tensor* $\mathbf{\Sigma}$ *is a random Gaussian field with zero mean and satisfying* (2.16)*. Then the radius* $R = R(t)$ *of the spherical charged molecule with a point charge* Q *at its center satisfies the generalized RP equation*

$$\rho_{\rm w}\left(R\ddot{R} + \frac{3}{2}\dot{R}^2\right) + \frac{4\mu_{\rm w}\dot{R}}{R} = F(R) + \xi \tag{3.6}$$

if the NSE (2.10) *is satisfied,*

$$\rho_{\rm w}\left(R\ddot{R} + 2\dot{R}^2\right) + \frac{4\mu_{\rm w}\dot{R}}{R} = F(R) + \xi \tag{3.7}$$

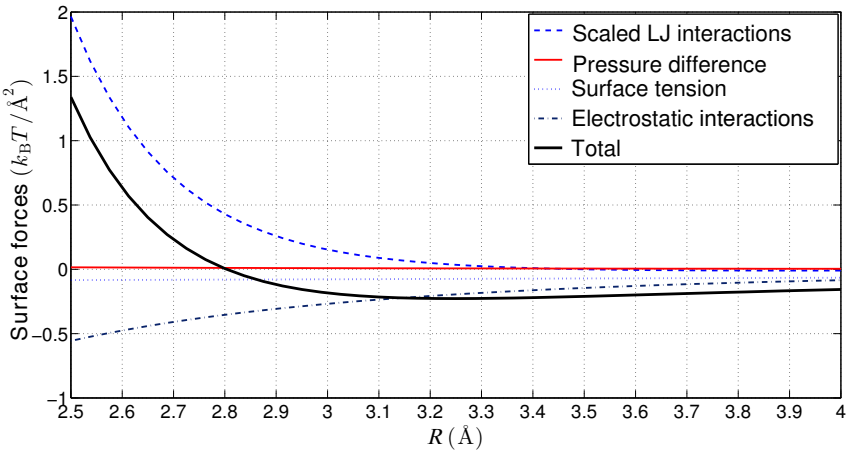

FIG. 2. *The total surface force density $F = F(R)$ with $U_{\text{ext}} = 0$ and all its components. The unique equilibrium radius is $R_{\text{eq}} = 2.8$ Å. The dominant components are the LJ interaction and electrostatic interaction forces.*

if the time-dependent Stokes equation (2.14) *is satisfied, or*

$$\frac{4\mu_{\text{w}}\dot{R}}{R} = F(R) + \xi \tag{3.8}$$

if the time-independent Stokes equation (2.15) *is satisfied, where $\xi = \xi(t)$ is a Gaussian white noise with*

$$\langle \xi(t)\xi(t')\rangle = \frac{4}{3}\mu_{\text{w}}k_{\text{B}}T\delta(t-t'). \tag{3.9}$$

We remark that each of the three versions of the generalized RP equation (3.6)–(3.8) is a SODE with a multiplicative noise. Note that only the macroscopic quantities, velocity, pressure, and electrostatic potential are assumed to be spherically symmetric. The stochastic stress tensor, however, is not assumed to be spherically symmetric.

The quantity $F(R)$ defined in (3.3) is the surface force density on the spherical boundary $r = R$. An equilibrium radius R_{eq} is determined by $F(R_{\text{eq}}) = 0$. This is exactly the governing equation in the static variational implicit-solvent model (for a single-atom spherical molecule); cf. [49, equation (II.8)] with $U_{\text{ext}} = 0$. In Figure 2, we plot this surface force density $F = F(R)$ with $U_{\text{ext}} = 0$, together with all its components: the pressure difference $P_0(R) - P_\infty$ (cf. (3.4)), the interfacial tension force $-2\gamma_0(H - \tau K) = -2\gamma_0(1/R - \tau/R^2)$, the scaled LJ interaction $n_{\text{w}}U_{\text{LJ}}$, and the electrostatic force $f_{\text{elec}}(R)$ (cf. (3.5)). The values of parameters P_∞, γ_0, τ, ε, σ, etc. are all listed in Table 1 below in section 4. Note that in this case there is only one equilibrium radius $R_{\text{eq}} = 2.8$ Å. Around this equilibrium radius, the main components of the force are the excluded-volume effect from the LJ part of the force and the electrostatic force. We see from (3.6)–(3.8) that the solvent fluid flow does not change this equilibrium [28].

Proof of Theorem 3.1. By the spherical symmetry, the velocity, pressure, and electrostatic potential are given by $\mathbf{u} = u(r,t)\mathbf{r}/r$ $(r > R(t))$, $P = P(r,t)$, and $\psi = \psi(r,t)$, respectively. Equation (2.9) of the incompressibility now becomes $r^{-2}\partial_r(r^2u) =$

0 for $r > R(t)$. Hence, $u(r,t) = C(t)/r^2$ for some $C(t)$. This and (2.8), which is now $\dot{R}(t) = u(R(t),t)$, then lead to $C(t) = R(t)^2\dot{R}(t)$ and further to

$$u(r,t) = \frac{R(t)^2\dot{R}(t)}{r^2} \qquad \text{for } r > R(t). \tag{3.10}$$

By the spherical symmetry and by dot producting both sides of the stochastic NSE (2.10), we obtain by a series of calculations that (cf. [5, 18])

$$\begin{aligned}&\rho_{\rm w}\left(\frac{\partial u}{\partial t} + u\frac{\partial u}{\partial r}\right)\\ &= \mu_{\rm w}\left[\frac{1}{r^2}\frac{\partial}{\partial r}\left(r^2\frac{\partial u}{\partial r}\right) - \frac{2u}{r^2}\right] - \frac{\partial P_{\rm w}}{\partial r} - n_{\rm w}U'_{\rm ext}(r) + (\nabla\cdot\boldsymbol{\Sigma})\cdot\frac{\mathbf{r}}{r} \qquad \forall r > R(t).\end{aligned} \tag{3.11}$$

With (3.10), we can verify that the term inside the brackets above vanishes. Hence, by (3.10) again, (3.11) becomes

$$\rho_{\rm w}\left(\frac{R^2\ddot{R} + 2R\dot{R}^2}{r^2} - \frac{2R^4\dot{R}^2}{r^5}\right) = -\frac{\partial P_{\rm w}}{\partial r} - n_{\rm w}U'_{\rm ext}(r) + (\nabla\cdot\boldsymbol{\Sigma})\cdot\frac{\mathbf{r}}{r} \qquad \forall r > R(t).$$

Integrating against r from $R = R(t)$ to the infinity, we further get by the assumption $U_{\rm ext}(\infty) = 0$ (cf. (3.2)) that

$$\rho_{\rm w}\left(R\ddot{R} + \frac{3}{2}\dot{R}^2\right) = P_{\rm w}(R) - P_\infty + n_{\rm w}U_{\rm ext}(R) + \int_R^\infty (\nabla\cdot\boldsymbol{\Sigma})\cdot\frac{\mathbf{r}}{r}\,dr. \tag{3.12}$$

By (2.11), the pressure inside the spherical solute, $P_{\rm p} = P_{\rm p}(R)$, is given by (3.4). Solving the linear PB equation (2.12) for the underlying one-atom system, where $B(\psi)$ is given in (2.7) and $\psi = 0$ at the infinity, we obtain explicitly the electrostatic potential [9]

$$\psi(r,t) = \begin{cases} \dfrac{Q}{4\pi\varepsilon_{\rm w}\varepsilon_0 R(1+\kappa R)} + \dfrac{Q}{4\pi\varepsilon_{\rm p}\varepsilon_0}\left(\dfrac{1}{r} - \dfrac{1}{R}\right) & \text{if } r < R,\\ \dfrac{Q}{4\pi\varepsilon_{\rm w}\varepsilon_0(1+\kappa R)}\cdot\dfrac{1}{r}e^{-\kappa(r-R)} & \text{if } r > R,\end{cases}$$

where again $R = R(t)$. Note that the mean and Gaussian curvatures on $\Gamma(t)$, which is defined by $r = R(t)$, are given by $H = 1/R(t)$ and $K = 1/R(t)^2$, respectively. By (2.6), the boundary force $-\delta_\Gamma G[\Gamma]$ on $\Gamma(t)$ is now a function of $R = R(t)$ and is given by

$$-\delta_\Gamma G[\Gamma(t)] = P_{\rm p}(R) - P_{\rm w}(R) - 2\gamma_0\left(\frac{1}{R} - \frac{\tau}{R^2}\right) + n_{\rm w}U_{\rm LJ}(R) + f_{\rm elec}(R),$$

where $f_{\rm elec}(R)$ is given exactly by (3.5).

Since $\mathbf{u} = u(r,t)\mathbf{r}/r$ with $u = u(r,t)$ given by (3.10), we have by a series of calculations that

$$\mathbf{D}(\mathbf{u})\mathbf{n}\cdot\mathbf{n} = \partial_r u = -\frac{2R^2\dot{R}}{r^3}.$$

It now follows from the above two equations that the force balance equation (2.13), with a dot product with $\mathbf{n}$, then becomes

$$-\frac{4\mu_{\rm w}\dot{R}}{R} + P_{\rm p}(R) - P_{\rm w}(R) - 2\gamma_0\left(\frac{1}{R} - \frac{\tau}{R^2}\right) + n_{\rm w}U_{\rm vdW}(R) + f_{\rm elec}(R) = 0.$$

This and (3.12) lead to

$$\rho_{\rm w}\left(R\ddot{R}+\frac{3}{2}\dot{R}^2\right)+\frac{4\mu_{\rm w}\dot{R}}{R}=F(R)+\int_R^\infty(\nabla\cdot\mathbf{\Sigma})\cdot\frac{\mathbf{r}}{r}\,dr, \tag{3.13}$$

where $F(R)$ is given in (3.3) and the potential $U_{\rm vdW}$ is replaced by $U_{\rm LJ}$ given in (3.1).

Note that if the velocity field $\mathbf{u}$ satisfies the time-dependent Stokes equation (2.14) instead of the NSE (2.10), then the term $u\partial_r u$ on the left-hand side of (3.11) should be dropped. Consequently, the term $(3/2)\dot{R}^2$ in (3.12) and (3.13) should be replaced by $2\dot{R}^2$. If the velocity field satisfies the time-independent Stokes equation (2.15), then the left-hand side of (3.11) is 0. Consequently, the term $\rho_{\rm w}(R\ddot{R}+(3/2)\dot{R}^2)$ in (3.12) and (3.13) should be set to 0.

We now consider the stochastic term in (3.13). The change of basis matrix from the Cartesian coordinates (x,y,z) to spherical coordinates (r,θ,ϕ), where θ is the polar angle $(0\le\theta\le\pi)$ and ϕ is the azimuthal angle $(0\le\phi<2\pi)$, is

$$A=\begin{bmatrix}\sin\theta\cos\phi & \sin\theta\sin\phi & \cos\theta\\ \cos\theta\cos\phi & \cos\theta\sin\phi & -\sin\theta\\ -\sin\phi & \cos\phi & 0\end{bmatrix}.$$

Thus, the stochastic stress tensor $\mathbf{\Sigma}$ in the Cartesian coordinates can be converted to that in the spherical coordinates with the formula

$$\begin{bmatrix}\Sigma_{rr} & \Sigma_{r\theta} & \Sigma_{r\phi}\\ \Sigma_{\theta r} & \Sigma_{\theta\theta} & \Sigma_{\theta\phi}\\ \Sigma_{\phi r} & \Sigma_{\phi\theta} & \Sigma_{\phi\phi}\end{bmatrix}=A\begin{bmatrix}\Sigma_{xx} & \Sigma_{xy} & \Sigma_{xz}\\ \Sigma_{yx} & \Sigma_{yy} & \Sigma_{yz}\\ \Sigma_{zx} & \Sigma_{zy} & \Sigma_{zz}\end{bmatrix}A^T, \tag{3.14}$$

where T denotes the matrix transpose. From this we obtain by a series of calculations that

$$\begin{aligned}\Sigma_{rr}&=(\sin\theta)^2(\cos\phi)^2\Sigma_{xx}+(\sin\theta)^2\sin\phi\cos\phi\,\Sigma_{yx}+\sin\theta\cos\theta\cos\phi\,\Sigma_{zx}\\&\quad+(\sin\theta)^2\sin\phi\cos\phi\,\Sigma_{xy}+(\sin\theta)^2(\sin\phi)^2\Sigma_{yy}+\sin\theta\cos\theta\cos\phi\,\Sigma_{zy}\\&\quad+\sin\theta\cos\theta\cos\phi\,\Sigma_{xz}+\sin\theta\cos\theta\sin\phi\,\Sigma_{yz}+(\cos\theta)^2\,\Sigma_{zz},\end{aligned} \tag{3.15}$$

$$\begin{aligned}\Sigma_{\theta\theta}&=(\cos\theta)^2(\cos\phi)^2\Sigma_{xx}+(\cos\theta)^2\sin\phi\cos\phi\,\Sigma_{yx}-\sin\theta\cos\theta\cos\phi\,\Sigma_{zx}\\&\quad+(\cos\theta)^2\sin\phi\cos\phi\,\Sigma_{xy}+(\cos\theta)^2(\sin\phi)^2\Sigma_{yy}-\sin\theta\cos\theta\sin\phi\,\Sigma_{zy}\\&\quad-\sin\theta\cos\theta\cos\phi\,\Sigma_{xz}-\sin\theta\cos\theta\sin\phi\,\Sigma_{yz}+(\sin\theta)^2\Sigma_{zz},\end{aligned} \tag{3.16}$$

$$\Sigma_{\phi\phi}=(\sin\phi)^2\Sigma_{xx}-\sin\phi\cos\phi\,\Sigma_{yx}-\sin\phi\cos\phi\,\Sigma_{xy}+(\cos\phi)^2\Sigma_{yy}. \tag{3.17}$$

By these and (3.14), we obtain the formula for the divergence $\nabla\cdot\mathbf{\Sigma}$ of the stochastic tensor $\mathbf{\Sigma}$ in the spherical coordinates

$$\begin{bmatrix}\frac{\partial\Sigma_{rr}}{\partial r}+2\frac{\Sigma_{rr}}{r}+\frac{1}{r}\frac{\partial\Sigma_{\theta r}}{\partial\theta}+\cot\theta\frac{\Sigma_{\theta r}}{r}+\frac{1}{r\sin\theta}\frac{\partial\Sigma_{\phi r}}{\partial\phi}-\frac{\Sigma_{\theta\theta}+\Sigma_{\phi\phi}}{r}\\ \frac{\partial\Sigma_{r\theta}}{\partial r}+2\frac{\Sigma_{r\theta}}{r}+\frac{1}{r}\frac{\partial\Sigma_{\theta\theta}}{\partial\theta}+\cot\theta\frac{\Sigma_{\theta\theta}}{r}+\frac{1}{r\sin\theta}\frac{\partial\Sigma_{\phi\theta}}{\partial\phi}+\frac{\Sigma_{\theta r}}{r}-\cot\theta\frac{\Sigma_{\phi\phi}}{r}\\ \frac{\partial\Sigma_{r\phi}}{\partial r}+2\frac{\Sigma_{r\phi}}{r}+\frac{\sin\theta}{r}\frac{\partial\Sigma_{\theta\phi}}{\partial\theta}+\cot\theta\frac{\Sigma_{\theta\phi}}{r}+\frac{1}{r\sin\theta}\frac{\partial\Sigma_{\phi\phi}}{\partial\phi}+\frac{\Sigma_{\phi r}+\Sigma_{\phi\theta}}{r}\end{bmatrix}.$$

By definition, the first row in this matrix, which may depend on θ and ϕ, is exactly $(\nabla\cdot\mathbf{\Sigma})\cdot\mathbf{r}/r$, i.e.,

$$(\nabla\cdot\mathbf{\Sigma})\cdot\frac{\mathbf{r}}{r}=\frac{\partial\Sigma_{rr}}{\partial r}+2\frac{\Sigma_{rr}}{r}+\frac{1}{r}\frac{\partial\Sigma_{\theta r}}{\partial\theta}+\cot\theta\frac{\Sigma_{\theta r}}{r}+\frac{1}{r\sin\theta}\frac{\partial\Sigma_{\phi r}}{\partial\phi}-\frac{\Sigma_{\theta\theta}+\Sigma_{\phi\phi}}{r}. \tag{3.18}$$

Note that all terms in (3.13), except the stochastic term, are independent of θ and ϕ. We can then consider the spherical averages of these terms. More precisely, if we multiply both sides of (3.13) by $\sin\theta/(4\pi)$ and then integrate against θ over $0 \le \theta \le \pi$ and against ϕ over $0 \le \phi \le 2\pi$, then we obtain the designed equation (3.6) with the noise term

$$\begin{aligned}\xi(t) &= \frac{1}{4\pi}\int_0^{2\pi}\int_0^{\pi}\int_R^{\infty} (\nabla\cdot\mathbf{\Sigma})\cdot\frac{\mathbf{r}}{r}\,\sin\theta\,dr\,d\theta\,d\phi \\ &= \frac{1}{4\pi}\int_0^{2\pi}\int_0^{\pi}\int_R^{\infty}\Big[\sin\theta\frac{\partial\Sigma_{rr}}{\partial r}+\frac{2\sin\theta}{r}\Sigma_{rr}+\frac{\sin\theta}{r}\frac{\partial\Sigma_{\theta r}}{\partial\theta} \\ &\qquad + \frac{\cos\theta}{r}\Sigma_{\theta r}+\frac{1}{r}\frac{\partial\Sigma_{\phi r}}{\partial\phi}-\frac{\sin\theta}{r}\left(\Sigma_{\theta\theta}+\Sigma_{\phi\phi}\right)\Big]\,dr\,d\theta\,d\phi, \end{aligned} \tag{3.19}$$

where the second equality follows from (3.18). Equation (3.6) is thus proved. Equations (3.7) and (3.8) are similarly proved; see the remark below (3.13).

We now show that $\xi(t)$ given in (3.19) is a zero-mean Gaussian field with the correlation (3.9). The third term, by integration by parts, is

$$\frac{1}{4\pi}\int_R^{\infty}\int_0^{2\pi}\int_0^{\pi}\frac{1}{r}\frac{\partial\Sigma_{\theta r}}{\partial\theta}\sin\theta\,d\theta\,d\phi\,dr = -\frac{1}{4\pi}\int_R^{\infty}\int_0^{2\pi}\int_0^{\pi}\frac{\Sigma_{\theta r}}{r}\cos\theta\,d\theta\,d\phi\,dr,$$

which is precisely the negation of the fourth term, so they cancel. The fundamental theorem of calculus, applied to the integration of the fifth term against ϕ, leads to a factor of $\Sigma_{\phi r}(r,\theta,2\pi)-\Sigma_{\phi r}(r,\theta,0)$, which vanishes as well due to the periodicity of ϕ. The second and last terms now also cancel due to the following integrals computed from (3.15)–(3.17):

$$\begin{aligned}\frac{1}{4\pi}\int_0^{2\pi}\int_0^{\pi}\sin\theta\,\Sigma_{rr}\,d\theta\,d\phi &= \frac{\Sigma_{xx}+\Sigma_{yy}+\Sigma_{zz}}{3}, \\ \frac{1}{4\pi}\int_0^{2\pi}\int_0^{\pi}\sin\theta\,\Sigma_{\theta\theta}\,d\theta\,d\phi &= \frac{\Sigma_{xx}+\Sigma_{yy}+4\Sigma_{zz}}{6}, \\ \frac{1}{4\pi}\int_0^{2\pi}\int_0^{\pi}\sin\theta\,\Sigma_{\phi\phi}\,d\theta\,d\phi &= \frac{\Sigma_{xx}+\Sigma_{yy}}{2}. \end{aligned} \tag{3.20}$$

We now only have the first term of the integral (3.19). By integration by parts, (3.20), and the fact that $\mathbf{\Sigma}$ vanishes at the infinity, we obtain

$$\begin{aligned}\xi(t) &= \frac{1}{4\pi}\int_0^{2\pi}\int_0^{\pi}\int_R^{\infty}\frac{\partial\Sigma_{rr}}{\partial r}\,dr\,\sin\theta\,d\theta\,d\phi \\ &= -\frac{1}{4\pi}\int_0^{2\pi}\int_0^{\pi}\Sigma_{rr}(R,\theta,\phi)\sin\theta\,d\theta\,d\phi \\ &= -\frac{1}{3}\left(\Sigma_{xx}+\Sigma_{yy}+\Sigma_{zz}\right)\Big|_{r=R(t)}. \end{aligned} \tag{3.21}$$

Notice that Σ_{xx}, Σ_{yy}, and Σ_{zz} are uncorrelated, zero-mean Gaussian random fields. Hence, $\xi(t)$ is a zero-mean Gaussian random field. By (2.16), the covariance of $-(\Sigma_{xx}+\Sigma_{yy}+\Sigma_{zz})/3$ is

$$\frac{1}{9}\langle\left(\Sigma_{xx}+\Sigma_{yy}+\Sigma_{zz}\right)(\mathbf{x},t)\left(\Sigma_{xx}+\Sigma_{yy}+\Sigma_{zz}\right)(\mathbf{x}',t')\rangle$$

$$= \frac{1}{9}\left[\langle \Sigma_{xx}(\mathbf{x},t)\ \Sigma_{xx}(\mathbf{x}',t')\rangle + \langle \Sigma_{yy}(\mathbf{x},t)\ \Sigma_{yy}(\mathbf{x}',t')\rangle + \langle \Sigma_{zz}(\mathbf{x},t)\ \Sigma_{zz}(\mathbf{x}',t')\rangle\right]$$
$$= \frac{4}{3}\mu_{\mathrm{w}} k_B T\, \delta(\mathbf{x}-\mathbf{x}')\,\delta(t-t').$$

Setting $\mathbf{x} = (R(t),0,0)$ and $\mathbf{x}' = (R(t'),0,0)$ in the above equation and noting that $R(t) = R(t')$ and $t = t'$ if and only if $t = t'$, we then obtain (3.9) by (3.21). ∎

4. Numerical methods and simulations. In this section, we design numerical methods to solve the generalized RP equation in all of its three versions. Let us first consider the second-order SODE (3.6) and (3.7). Since $\xi(t)$ is a white noise with the correlation (3.9), formally we have $\xi\, dt = \sqrt{4\mu_{\mathrm{w}} k_B T/3}\, dw_t$, where w_t denotes the standard Wiener process with zero mean and the delta correlation. Those two equations (3.6) and (3.7) can then be written as a system of first-order SODEs in Itô differential form as

$$dX_t = A(X_t)\, dt + B(X_t)\, dW_t,$$

where

$$X_t = \begin{bmatrix} R \\ \dot{R} \end{bmatrix},\ A(X_t) = \begin{bmatrix} \dot{R} \\ -\left(\frac{\alpha}{R} + \frac{4\mu_{\mathrm{w}}}{\rho_{\mathrm{w}} R^2}\right)\dot{R} + \frac{F(R)}{\rho_{\mathrm{w}} R} \end{bmatrix},$$
$$B(X_t) = \begin{bmatrix} 0 & 0 \\ 0 & \frac{\sqrt{\frac{4}{3}\mu_{\mathrm{w}} k_B T}}{\rho_{\mathrm{w}} R} \end{bmatrix},\ W_t = \begin{bmatrix} 0 \\ w_t \end{bmatrix}.$$

Here, $\alpha = 2$ for (3.6) and $\alpha = 3/2$ for (3.7), respectively.

We partition the time axis into intervals of width Δt and set $X^{(0)} = X_0$ and $X^{(n)}$ an approximation to X_{t_n}, where $t_n = n\Delta t$ $(n = 1, 2, \dots)$. Denote by A_i, X_i, $X_i^{(n)}$ the ith component of the vector A, X, and $X^{(n)}$, respectively, and by B_{ij} the (i,j)-entry of the matrix B. Applying the multidimensional Milstein method [23], we obtain the following scheme for the components of $X^{(n)}$:

$$X_i^{(n+1)} = X_i^{(n)} + A_i(X^{(n)})\Delta t + \sum_{j=1}^{2} B_{ij}(X^{(n)})\Delta W_j^{(n)}$$
$$+ \frac{1}{2}\sum_{j,k,\ell=1}^{2} \frac{\partial B_{ij}}{\partial X_\ell}(X^{(n)}) B_{\ell k}(X^{(n)}) \left[\Delta W_j^{(n)} \Delta W_k^{(n)} - \Delta t\, \sigma_{jk} - S_{jk}^{(n)}\right], \tag{4.1}$$
$$i = 1, 2,$$

where $\Delta W^{(n)}$ are vectors of independent and identically distributed Gaussian random variables with mean zero and variance Δt, (σ_{jk}) is the correlation matrix for W_t, and $S_{jk}^{(n)}$ are the "Lévy areas" defined by

$$S_{jk}^{(n)} = \int_{t_n}^{t_{n+1}} [(W_t)_j - (W_{t_n})_j]\, dW_k - \int_{t_n}^{t_{n+1}} [(W_t)_k - (W_{t_n})_k]\, dW_j.$$

Due to the special structure of the matrix B, the second sum in (4.1) vanishes. Hence, the scheme (4.1) simplifies to the Euler–Maruyama scheme, i.e.,

$$X_1^{(n+1)} = X_1^{(n)} + X_2^{(n)}\Delta t, \tag{4.2}$$
$$X_2^{(n+1)} = X_2^{(n)} + A_2(X^{(n)})\Delta t + B_{22}(X^{(n)})\Delta W_2^{(n)}. \tag{4.3}$$

TABLE 1
Parameters for the generalized RP equations.

Parameter	Symbol	Value	Unit
temperature	T	298	K
solvent dynamic viscosity	μ_{w}	0.2	$\mathrm{k_B T \cdot ps/\AA^3}$
solvent number density	n_{w}	0.0333	$\mathrm{\AA^{-3}}$
solvent mass density	ρ_{w}	2.42×10^{-3}	$\mathrm{k_B T \cdot ps^2/\AA^5}$
bulk solvent pressure	P_∞	2.46×10^{-5}	$\mathrm{k_B T/\AA^3}$
surface tension	γ_0	0.175	$\mathrm{k_B T/\AA^2}$
Tolman length	τ	1	Å
LJ length parameter	σ	3.5	Å
LJ energy parameter	ε	0.3	$\mathrm{k_B T}$
vacuum permittivity	ε_0	1.4372×10^{-4}	$\mathrm{e^2/(k_B T \cdot \AA)}$
solute dielectric constant	ε_{p}	1	
solvent dielectric constant	ε_{w}	78	
inverse Debye length	κ	0.025	$\mathrm{\AA^{-1}}$
point charge	Q	1	e

Similarly, we can rewrite the SODE (3.8) in Itô's form for $R_t = R(t)$ as

$$dR_t = a(R_t)\,dt + b(R_t)\,dw_t, \tag{4.4}$$

where

$$a(R_t) = \frac{RF(R)}{4\mu_{\mathrm{w}}} \qquad \text{and} \qquad b(R_t) = \sqrt{\frac{k_{\mathrm{B}}T}{12\mu_{\mathrm{w}}}}\,R.$$

We partition the time axis into intervals of width Δt and set $R^{(n)}$ an approximation to R_{t_n}, where $t_n = n\Delta t$ $(n = 1, 2, \dots)$. We use the Euler–Maruyama scheme [23] to discretize (4.4),

$$R^{(n+1)} = R^n + a(R^n)\Delta t + b(R^n)\Delta w^n, \tag{4.5}$$

where Δw^n are independent and identically distributed Gaussian random variables with mean zero and variance Δt.

For our numerical solutions to the generalized RP equations, we use the parameters listed in Table 1. Note that the inverse Debye length κ (cf. (2.7)) is slightly larger than 0.029, which is estimated with $M = 2$, $q_1 = 1$, $q_2 = -1$, $c_1^\infty = c_2^\infty = 0.1$M. In our simulations for each of the three versions (3.6), (3.7), and (3.8) of the generalized RP equation, we choose $\Delta t = 10^{-3}$ picoseconds and run 10^6 steps. We collect the histogram data of the simulated radius $R(t)$ and use the Gaussian convolution to filter the histogram.

In Figure 3, we plot the probability distribution of the simulated radius for each of the three equations. From the results, we see that the probability distributions of the radius obtained by the three different versions of the generalized RP equation are almost the same. The difference of these equations is in the timescale. Note that the peak of each of the distributions corresponds to the optimal radius, which is very close to but not exactly the same as the equilibrium radius R_{eq} defined by $F(R_{\mathrm{eq}}) = 0$ with $F(R)$ given in (3.3). This indicates that, in terms of the description of the stochastic effect to the radius, the simple time-independent Stokes equation can be used.

5. Application: The effective radius of a single ion. In this section, we study the effective radius of a single ion immersed in an aqueous solvent by MD simulations and our generalized RP equation.

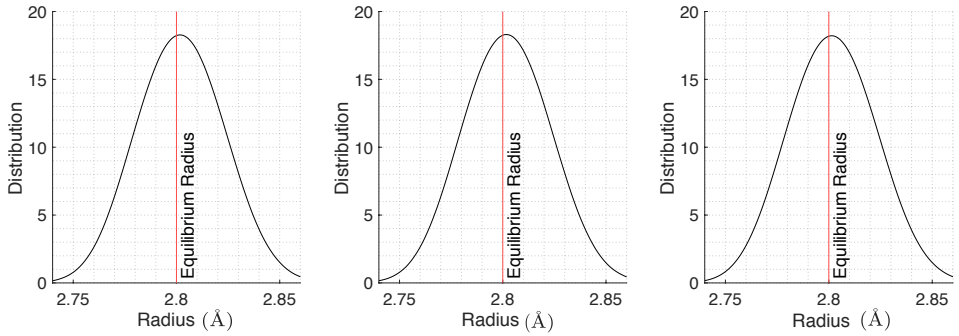

FIG. 3. *The probability distribution of the radius $R = R(t)$ obtained from the simulation of the generalized RP equation* (3.7) *(left),* (3.7) *(middle), and* (3.8) *(right). The vertical line in each plot shows the equilibrium radius defined by $F(R) = 0$ with $F(R)$ given in* (3.3).

We use the GROMACS MD simulations package with the SPC/E water model and OPLS/AA force field. We also use particle mesh Ewald summation for the calculation of electrostatic interactions. The temperature is set to be $T = 298\,\mathrm{K}$, and the simulation box is a cube of size around 50 Å × 50 Å × 50 Å. At the center of this box, we place an artificial ion of point charge Q with $Q = +1$, -1, $+2$, or -2. We also place around 4,050 water molecules and a few Na^+ and Cl^- ions in the simulation box. The ion-water LJ parameters are fixed to be $\sigma = 3.5$ Å and $\varepsilon = 0.3\ k_B T$. In each simulation, we run for 1,000,000–10,000,000 time steps with each step of 1 femtosecond.

Figure 4 shows the radial distribution of the water molecules around the ion obtained from our MD simulations. From such a distribution, we can extract four different radii of the ion as illustrated in the subplot (a):

(1) the "first nonzero" radius, marked by × on the horizontal axis in subplot (a), defined to be the first distance to the center of the ion at which the distribution is nonzero
(2) the "peak" radius, defined to be the distance to the center of the ion at which the distribution reaches its first maximum
(3) the "half peak" radius, defined to be the distance to the center of the ion at which the distribution reaches half of its first peak value
(4) the "bulk" radius, defined to be the distance at which the distribution reaches the bulk value for the first time

We also solve the generalized RP equation (3.8) with the same parameters as those in the MD simulations and others in Table 1. We record in Table 2 all the four radii defined from the radial distribution of water around the ion and the radius determined by the generalized RP equation for all the four ions (defined by the four Q values).

We observe from Table 2 that the SODE radius for each of the anions (with negative Q value) is larger than any of those radii defined from the water distribution, while the SODE radius is always smaller than those defined from such distributions for cations (with positive Q value). The SODE does not distinguish the sign of charge Q. This is known to be an issue of the continuum electrostatic model, which is unable to capture the charge asymmetry [19]. However, the SODE radius approximates very well the averaged peak radius over those for the two ions with the same amount of charge (same absolute value of Q), i.e., average over $Q = +1$ and $Q = -1$ or over $Q = +2$ and $Q = -2$. In general, the SODE radius approximates those of cations

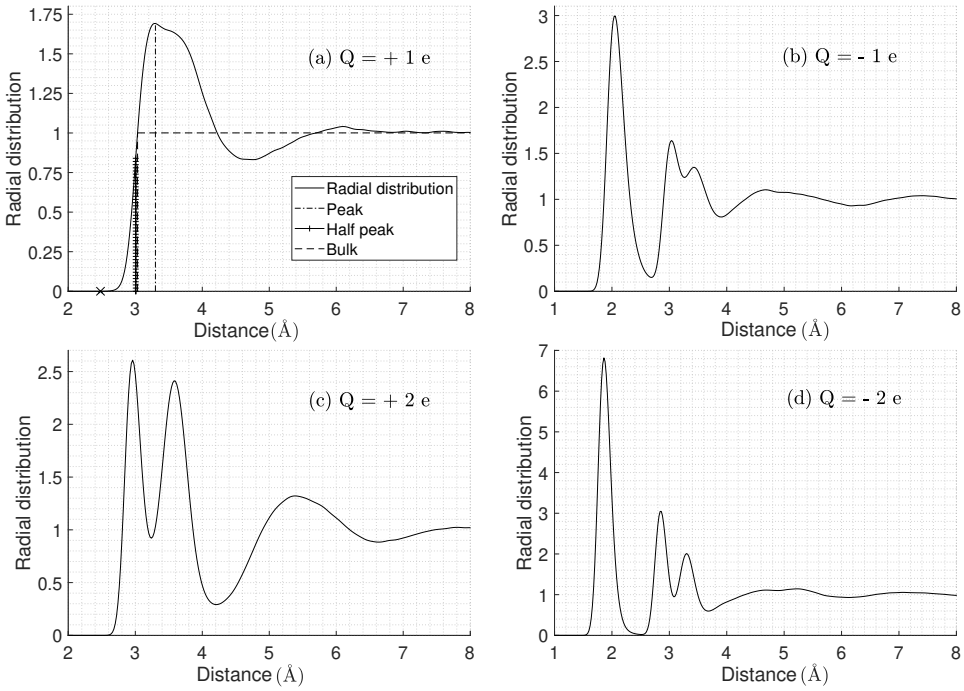

FIG. 4. *The radial distribution of water molecules around an artificial ion carrying the point charge Q: In* (a)*, the dash-dotted line, broken line, and the line with symbol + are used to define the peak, half peak, and bulk values of water distribution. The cross sign × between* 2 *and* 3 *on the horizontal axis of* (a) *defines the first point of distance to the center of the ion with a nonzero distribution.*

TABLE 2

Effective ionic radii determined by the radial distribution of water from MD simulations (first nonzero, peak, half peak, and bulk) and by the generalized RP equation (3.8) *for four artificially designed ions.*

Ion	Q (e)	First nonzero (Å)	Peak (Å)	Half peak (Å)	Bulk (Å)	RP (Å)
1	1	2.48	3.32	3.00	3.03	2.80
2	−1	1.56	2.04	1.90	1.86	2.80
3	2	2.32	2.96	2.83	2.81	2.46
4	−2	1.46	1.86	1.74	1.67	2.46

better than anions. A good value of the effective radius for an anion will be the SODE radius minus 0.5 Å.

6. Conclusions. We have introduced a dynamic implicit-solvent model to describe the conformational dynamics of charged molecules in a fluctuating solvent fluid. Key in such a model is the stochastic Stokes equation for solvent fluid, neglecting the inertia, which is rather weak at the molecular scale, and the balance of the viscous force, hydrostatic pressure, surface tension force, electrostatic force, and vdW interaction force at the solute-solvent interface. Within such a framework, we have derived the generalized RP equation for a spherical molecule and used the equation, together with MD simulations, to determine an effective radius of a single ion. Our numerical results indicate that the fluctuation-dissipation balance is reached for the generalized

RP equation. Although this stochastic differential equation is only for a spherical molecule, it can be used to test theories and methods for more complex systems and can also used for further mathematical analysis.

We use the dielectric PB equation, linear or nonlinear, to describe the electrostatics of an underlying molecular system. In our generalized RP equation for the radius of an ion in aqueous, we use the linear PB equation, for which we are able to obtain an analytical formula of the exact solution. In general, one needs to solve numerically the linear or nonlinear PB equation, with the latter being more computationally costly but also more accurate in describing the underlying electrostatic potential, particularly if the bulk ionic concentrations are not very low. In using the PB equation, we have implicitly assumed that the ionic charge relaxation is faster than the solvent fluid motion, which will affect the dynamics of the solute-solvent interface. For a near-equilibrium system, this is reasonable. Otherwise, the system of Poisson–Nernst–Planck equations for electrodiffusion of ions, with the dielectric boundary, is suggested to replace the dielectric PB equation.

There are several aspects of our dynamic implicit-solvent modeling framework that need to be improved. First, the pressure inside charged solutes can be important in molecular conformational changes [37, 42]. The ideal gas law used in our model for such pressure needs to be further tested and improved. Second, the fluctuation of the solute-solvent interface should be included in addition to the solvent fluctuation, as both are crucial to the molecular dynamics. Third, to capture the solute molecular mechanical interactions that are of critical importance in biological processes, it will be necessary to couple the solvent fluid motion with the solute molecular dynamics as is done in the variational model [12]. Fourth, experiments and MD simulations have indicated that the solvent shear flow can induce protein conformational changes [1, 30, 38, 41, 43, 48]. Since in general the tangential component of the velocity of a moving surface will not contribute to the motion of such a surface, modeling the shear flow around a solute-solvent interface remains challenging. Finally, efficient methods within the modeling framework should be developed for computing the free energy of an underlying molecular system.

Acknowledgments. We thank Professor Joachim Dzubiella, Dr. Yuen-Yick Kwan, Professor Ray Luo, Professor Hui Sun, and Professor Shenggao Zhou for many helpful discussions.

REFERENCES

[1] A. Alexander-Katz, M. F. Schneider, S. W. Schneider, A. Wixforth, and R. R. Netz, *Shear-flow-induced unfolding of polymeric globules*, Phys. Rev. Lett., 97 (2006), 138101.

[2] A. Ansari, C. M. Jones, E. R. Henry, J. Hofrichter, and W. A. Eaton, *The role of solvent viscosity in the dynamics of protein conformational changes*, Science, 256 (1992), pp. 1796–1798.

[3] G. K. Batchelor, *An Introduction to Fluid Dynamics*, Cambridge University Press, Cambridge, 1967.

[4] D. Beece, L. Eisenstein, H. Frauenfelder, D. Good, M. C. Marden, L. Reinisch, A. H. Reynolds, L. B. Sorensen, and K. T. Yue, *Solvent viscosity and protein dynamics*, Biochemistry, 19 (1980), pp. 5147–5157.

[5] C. E. Brennen, *Cavitation and Bubble Dynamics*, Oxford University Press, Oxford, 1995.

[6] Q. Cai, X. Ye, and R. Luo, *Dielectric pressure in continuum electrostatic solvation of biomolecules*, Phys. Chem. Chem. Phys., 14 (2012), pp. 15917–15925.

[7] Q. Cai, X. Ye, J. Wang, and R. Luo, *Dielectric boundary forces in numerical Poisson–Boltzmann methods: Theory and numerical strategies*, Chem. Phys. Lett., 514 (2011), pp. 368–373.

[8] J. Che, J. Dzubiella, B. Li, and J. A. McCammon, *Electrostatic free energy and its variations in implicit solvent models*, J. Phys. Chem. B, 112 (2008), pp. 3058–3069.
[9] H.-B. Cheng, L.-T. Cheng, and B. Li, *Yukawa-field approximation of electrostatic free energy and dielectric boundary force*, Nonlinearity, 24 (2011), pp. 3215–3236.
[10] L.-T. Cheng, J. Dzubiella, J. A. McCammon, and B. Li, *Application of the level-set method to the implicit solvation of nonpolar molecules*, J. Chem. Phys., 127 (2007), 084503.
[11] L.-T. Cheng, B. Li, and Z. Wang, *Level-set minimization of potential controlled Hadwiger valuations for molecular solvation*, J. Comput. Phys., 229 (2010), pp. 8497–8510.
[12] L.-T. Cheng, Y. Xie, J. Dzubiella, J. A. McCammon, J. Che, and B. Li, *Coupling the level-set method with molecular mechanics for variational implicit solvation of nonpolar molecules*, J. Chem. Theory Comput., 5 (2009), pp. 257–266.
[13] M. E. Davis and J. A. McCammon, *Electrostatics in biomolecular structure and dynamics*, Chem. Rev., 90 (1990), pp. 509–521.
[14] J. Dzubiella, *Interface dynamics of microscopic cavities in water*, J. Chem. Phys., 126 (2007), 194504.
[15] J. Dzubiella, J. M. J. Swanson, and J. A. McCammon, *Coupling hydrophobicity, dispersion, and electrostatics in continuum solvent models*, Phys. Rev. Lett., 96 (2006), 087802.
[16] B. Eisenberg, Y. K. Hyon, and C. Liu, *Energy variational analysis of ions in water and channels: Field theory for primitive models of complex ionic fluids*, J. Chem. Phys., 133 (2011), 04104.
[17] I. J. Finkelstein, A. M. Massari, and M. D. Fayer, *Viscosity-dependent protein dynamics*, Biophys. J., 92 (2007), pp. 3652–3662.
[18] S. Fujikawa, T. Yano, and M. Watanabe, *Vapor-Liquid Interfaces, Bubbles and Droplets: Fundamentals and Applications*, Springer-Verlag, Berlin, 2011.
[19] A. Grossfield, *Dependence of ion hydration on the sign of the ion's charge*, J. Chem. Phys., 122 (2005), 024506.
[20] S. J. Hagen, *Solvent viscosity and friction in protein folding dynamics*, Curr. Protein Pept. Sci., 11 (2010), pp. 385–395.
[21] D. D. Joseph and Y. Y. Renardy, *Fundamentals of Two-Fluid Dynamics, Part* I: *Mathematical Theory and Applications*, Springer-Verlag, Berlin, 1993.
[22] D. K. Klimov and D. Thirumalai, *Viscosity dependence of folding rates of protein*, Phys. Rev. Lett., 79 (1997), pp. 317–320.
[23] P. E. Kloeden and E. Platen, *Numerical Solution of Stochastic Differential Equations*, Springer-Verlag, Berlin, 1995.
[24] L. D. Landau and E. M. Lifshitz, *Fluid Mechanics*, Course of Theoretical Physics 6, Pergamon, 1959.
[25] Y. Levy and J. N. Onuchic, *Water mediation in protein folding and molecular recognition*, Annu. Rev. Biophys. Biomol. Struct., 35 (2006), pp. 389–415.
[26] B. Li, *Minimization of electrostatic free energy and the Poisson–Boltzmann equation for molecular solvation with implicit solvent*, SIAM J. Math. Anal., 40 (2009), pp. 2536–2566.
[27] B. Li., X.-L. Cheng, and Z.-F. Zhang, *Dielectric boundary force in molecular solvation with the Poisson–Boltzmann free energy: A shape derivative approach*, SIAM J. Appl. Math., 71 (2011), pp. 2093–2111.
[28] B. Li, H. Sun, and S. Zhou, *Stability of a cylindrical solute-solvent interface: Effect of geometry, electrostatics, and hydrodynamics*, SIAM J. Appl. Math., 73 (2015), pp. 907–928.
[29] F. Lugli and F. Zerbetto, *Molecular dynamics of nanobubbles' collapse in ionic solutions*, ChemPhysChem, 8 (2007), pp. 47–49.
[30] Y.-F. Maa and C. C. Hsu, *Protein denaturation by combined effect of shear and air-liquid interface*, Biotechnol. Bioeng., 54 (1997), pp. 503–512.
[31] R. E. Meyer, *Introduction to Mathematical Fluid Dynamics*, Dover, New York, 1982.
[32] M. Moseler and U. Landman, *Formation, stability, and breakup of nanojets*, Science, 289 (2000), pp. 1165–1169.
[33] M. S. Plesset, *The dynamics of cavitation bubbles*, J. Appl. Mech., 16 (1949), pp. 277–282.
[34] M. S. Plesset and A. Prosperetti, *Bubble dynamics and cavitation*, Annu. Rev. Fluid Mech., 9 (1977), pp. 145–185.
[35] A. Prosperetti, *Boundary conditions at a liquid-vapor interface*, Meccanica, 14 (1979), pp. 34–47.
[36] L. Rayleigh, *On the pressure developed in a liquid during the collapse of a spherical cavity*, Philos. Mag., 34 (1917), pp. 94–98.
[37] J. Roche, J. A. Caro, D. R. Norberto, P. Barthe, C. Roumestand, J. L. Schlessman, A. E. Garcia, B. G.-M. E, and C. A. Royer, *Cavities determine the pressure unfolding of proteins*, Proc. Natl. Acad. Sci. USA, 109 (2012), pp. 6945–6950.

[38] S. W. Schneider, S. Nuschele, A. Wixforth, C. Gorzelanny, A. Alexander-Katz, R. R. Netz, and M. F. Schneider, *Shear-induced unfolding triggers adhesion of von Willebrand factor fibers*, Proc. Natl. Acad. Sci. USA, 104 (2007), pp. 7899–7903.

[39] A. Sekhar, M. P. Latham, P. Vallurupalli, and L. E. Kay, *Viscosity-dependent kinetics of protein conformational exchange: Microviscosity effects and the need for a small viscogen*, J. Phys. Chem. B, 118 (2014), pp. 4546–4551.

[40] K. A. Sharp and B. Honig, *Electrostatic interactions in macromolecules: Theory and applications*, Annu. Rev. Biophys. Biophys. Chem., 19 (1990), pp. 301–332.

[41] C. A. Siedlecki, B. J. Lestini, K. K. Kottke-Marchant, S. J. Eppell, D. L. Wilson, and R. E. Marchant, *Shear-dependent changes in the three-dimensional structure of human von Willebrand factor*, Blood, 88 (1996), pp. 2939–2950.

[42] J. L. Silva and G. Weber, *Pressure stability of proteins*, Annu. Rev. Phys. Chem, 44 (1993), pp. 89–113.

[43] I. Singh, E. Themistou, L. Porcar, and S. Neelamegham, *Fluid shear induces conformation change in human blood protein von Willebrand factor in solution*, Biophys. J., 96 (2009), pp. 2313–2320.

[44] H. Sun, S. Zhou, L.-T. Cheng, and B. Li, *Numerical methods for solvent Stokes flow and solute-solvent interfacial dynamics of charged molecules*, J. Comput. Phys., 374 (2018), pp. 533–549.

[45] H. Sun, S. Zhou, D. K. Moore, L.-T. Cheng, and B. Li, *Numerical treatment of Stokes solvent flow and solute-solvent interfacial dynamics for nonpolar molecules*, J. Sci. Comput., 67 (2016), pp. 705–723.

[46] P. Szymczak and M. Cieplak, *Hydrodynamic effects in proteins*, J. Phys. Condensed Matter, 23 (2011), 033102.

[47] R. C. Tolman, *The effect of droplet size on surface tension*, J. Chem. Phys., 17 (1949), pp. 333–337.

[48] R. M. A. Vergauwe, H. Uji-i, K. D. Ceunynck, J. Vermant, K. Vanhoorelbeke, and J. Hofkens, *Shear-stress-induced conformational changes of von Willebrand factor in water-glycerol mixture observed with single molecule microscopy*, J. Phys. Chem. B, 118 (2014), pp. 5660–5669.

[49] Z. Wang, J. Che, L.-T. Cheng, J. Dzubiella, B. Li, and J. A. McCammon, *Level-set variational implicit solvation with the Coulomb-field approximation*, J. Chem. Theory Comput., 8 (2012), pp. 386–397.

[50] M. White, *Mathematical Theory and Numerical Methods for Biomolecular Modeling*, Ph.D. thesis, University of California, San Diego, 2013.

[51] L. Xiao, Q. Cai, Z. Li, H. Zhao, and R. Luo, *A multi-scale method for dynamics simulation in continuum solvent models.* I: *Finite-difference algorithm for Navier–Stokes equation*, Chem. Phys. Lett., 616–617 (2014), pp. 67–74.

[52] S. Zhou, L.-T. Cheng, J. Dzubiella, B. Li, and J. A. McCammon, *Variational implicit solvation with Poisson–Boltzmann theory*, J. Chem. Theory Comput., 10 (2014), pp. 1454–1467.

[53] S. Zhou, R. G. Weiss, L.-T. Cheng, J. Dzubiella, J. A. McCammon, and B. Li, *Variational implicit-solvent predictions of the dry-wet transition pathways for ligand-receptor binding and unbinding kinetics*, Proc. Natl. Acad. Sci. USA, 116 (2019), pp. 14989–14994.